Designing and building a pre-dispersive DMD spectrometer

Johan Karlander

LRAP431

February 14, 2011

Abstract

In this Master's thesis, a pre-dispersive DMD-based spectrometer has been designed and built. The aim was to create a demonstration setup to show how a digital micromirror device (DMD) can be used in spectroscopy. The DMD was placed at the image point of a spectrum created by a concave, reflective grating to direct certain wavelength components of the incoming light into an optical fiber. This can be used in combination with a single, large detector in the long wave near infrared region (1100-2500 nm) as a cost effective and robust hand held alternative to scanning monochromators and diode array spectrometers. It was shown that a multiplexing method, Hadamard spectroscopy, could be implemented to increase the signal-to-noise ratio without modifying the setup.

Contents

List of Figures

List of Tables

Chapter 1

Introduction

This master thesis was done at the division of Atomic Physics at Lund University in cooperation with the Danish company FOSS. The research at the Division of Atomic Physics is mainly laser based spectroscopy, using lasers from small diode lasers to a terrawatt laser system. FOSS designs, assembles and sells spectroscopic equipment. FOSS has mainly clients within agricultural, food, chemical and pharmaceutical industries. It has about 1150 employees around the world, but mainly in Denmark and Sweden [1].

In this master thesis a robust pre-dispersive spectrometer with a fixed grating was designed and built for demonstration purposes. The spectrometer uses a digital micromirror device (DMD) after the grating for wavelength selection, in combination with a large detector, instead of an array of detector elements. The spectrometer was designed for near infrared light (850-1000 nm). The aim of the thesis was to evaluate the DMD spectrometer with the prospect of developing a handheld device for longer wavelength operation.

In the long wave, near infrared region (1100-2500 nm) detector arrays are too expensive for many commercial applications. A more affordable solution is a scanning monochromator where the grating is turned by a motor. The high demands on reproducibility and consistency in speed on the grating rotation make it difficult to integrate a scanning monochromator in a handheld device. A DMD-based spectrometer is cost-effective and robust since it has no heavy moving parts.

The DMD is an important part of the spectrometer. A DMD is an array of small mirrors (typically 10x10 μm) where the angle of each mirror can be set digitally to reflect light in two possible directions. These devices can be found in applications such as projectors, medical science, optical networks and spectroscopy. The micromirrors can be set in a very short time which gives a high acquisition speed. The micromirrors can be set in a number of different configurations, which adds flexibility and opens up for possibilities such as Hadamard spectroscopy.

In Chapter 2 a short theoretical introduction to spectrometers is given. Their different components are explained as well as Hadamard spectroscopy, a method

for multiplexing. The emphasis in this chapter is on spectrometer designs containing a concave reflecting grating. In Chapter 3 the spectrometer, designed and built in this project, is presented. Different theoretical aspects are discussed for this special case. In chapter 4, results showing the performance and limitations are presented. Chapter 5 discusses how some problems encountered could be circumvented. In addition appendixes, A and B contain an alternative spectrometer design and aberration theory.

Chapter 2

Theory

2.1 Spectrometers

In a conventional, dispersive spectrometer, the different wavelength components of the analysed light are separated spatially by a grating or prism. In addition, imaging optics (mirrors or lenses) are used to collect and collimate light. Usually a narrow entrance slit is imaged on a detector. The position of the image depend on the wavelength of the light. In a scanning monochromator the detector is replaced by an exit slit (see figure 2.1). The wavelength is then changed by rotating the grating. A monochromator can be used either pre-dispersively (light source - spectrometer - sample - detector analyser) or post-dispersively (light source - sample - spectrometer - detector analyser). This design is often used in wavelength regions where semiconductor detector arrays are expensive. In a diode array (1D or 2D) spectrometer each diode element measures a subset of the total wavelength range. Such a design can only be used post-dispersively.

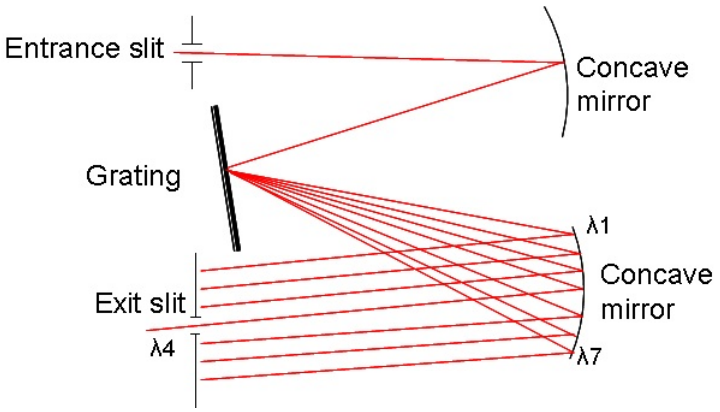

Figure 2.1: A monochromator set in a Czerny-Turner design. A diode array spectrometer could use the same setup where the exit slit has been exchanged with a detector array (such as a CCD).

2.2 Gratings

A grating divides light into its different wavelength components spatially according to figure 2.2. The incoming light at each groove has a slightly different path length which depends on the incident angle α and the outgoing angle β. The intensity reaches a maximum when constructive interference occurs, i.e. when the path difference ($\Delta L = \Delta L_1 - \Delta L_2$) between two diffracted rays is a whole number of wavelengths [6],

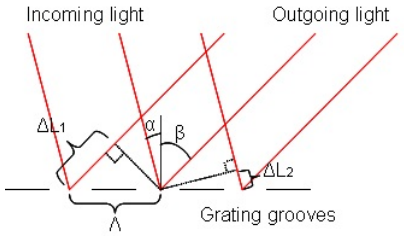

Figure 2.2: Principle of grating.

$$\Delta L = \Delta L_1 - \Delta L_2 = \Lambda sin(\alpha) + \Lambda sin(\beta) = k\lambda \tag{2.1}$$

where k is the order of diffraction and λ is the wavelength. In a scanning monochromator α and β changes when the grating is turned, but the sum remains constant. For a diode array spectrometer α remains constant while β varies with wavelength. Since the dispersion from a grating is a diffraction phenomenon the resolution depends on how many sources (i.e. grooves for a grating) that contribute to the constructive or destructive interference. A large grating with many illuminated grooves has a sharper diffraction pattern than a small grating. The resolving power, $R_{resolve}$, of a grating is [6]:

$$R_{resolve} = \frac{\lambda}{\partial\lambda} = \frac{kW_g}{\Lambda} \tag{2.2}$$

where $\partial\lambda$ is the smallest wavelength distance between two resolvable peaks and W_g is the width of the illuminated grating. There are two common types of gratings; Ruled gratings are made by mechanically etching out the grooves using a ruling engine. The second type, holographic gratings, are produced by using the interference fringe pattern from the standing wave produced by two laser beams [3]. Because of the production procedures the two types have different properties. Ruled gratings have a constant groove distance Λ. In a holographic gratings the groove density can be varied across the grating, creating effects such as high-order discrimination and considerably less stray light (usually a factor ten less than ruled gratings). Periodic ruling errors are not present in holographic gratings but can be a problem with ruled gratings. An advantage with ruled gratings is that they are easier to blaze[1] than holographic gratings [12].

[1] A blazed grating usually has triangular shaped grooves which tilt to increase the efficiency for a certain wavelength region (at the cost of lower efficiency in other regions).

2.3 Imaging

Most gratings are flat and need some optical component to collect light from the entrance slit, collimate and direct it towards the grating. The light is then focussed on the exit slit/detector elements by additional optics. Concave mirrors are most often used since they have no chromatic effects. Another option is to use a reflecting, concave grating which can image the entrance slit onto the detector array or exit slit (see figure 2.3) without additional optics.

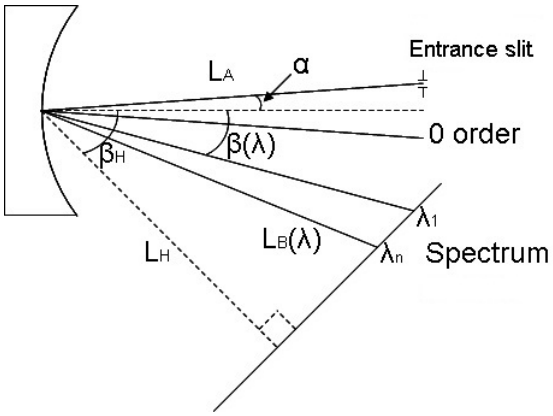

Figure 2.3: A holographic, concave, reflecting grating images the entrance slit onto the detector array (or exit slit depending on spectrometer). The length L_H and angle β_H decide at which distance and angle the plane of focus is located.

The image of each wavelength component is separated according to equation 2.1. A commonly used criteria to when two near lying components can be resolved is that they intersect beneath their half power point (see figure 2.4) [5].

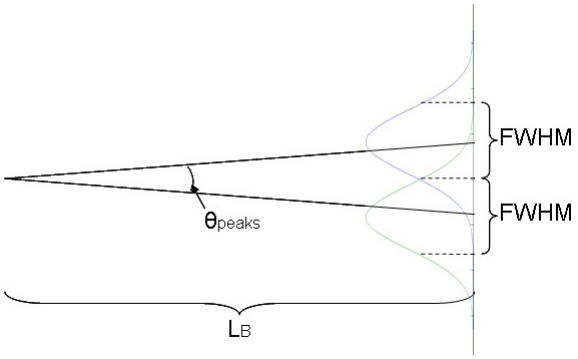

Figure 2.4: Two peaks can be resolved if they intersect at a value lower than the FWHM.

The separation angle between two peaks θ_{peaks} corresponds to a wavelength region at the spectrum (at length L_B). This can be calculated,

$$L_B \theta_{peaks} \frac{\partial \lambda}{\partial x} \geq FWHM \tag{2.3}$$

where $\frac{\partial \lambda}{\partial x}$ is the dispersion and the angle θ_{peaks} is small. The FWHM of a thin, spectral line appears broader to the instrument because of the grating, but also because of the width of the entrance slit and exit slit/detector array element size, diffraction and imaging errors. Together all these factors will set a lower limit to the FWHM.

2.3.1 Slits

The width of the entrance slit and exit slit/detector array elements in a spectrometer are important factors which limit both the resolution and light intensity through the device. Theoretically this can be modelled by convoluting the image of the entrance slit with the exit slit/detector elements (see figure 2.5). In figure 2.3 the entrance slit will be magnified $M = L_B/L_A$ times.

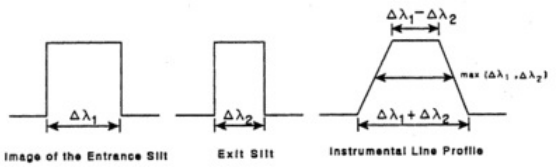

Figure 2.5: The resulting spectrum depends on the convolution of the image of the entrance slit and the exit slit [12].

When designing a spectrometer the size of the exit slit might vary. In a scanning monochromator solution, where one detector is used and the grating is turned, the size of the exit slit has little effect on the resolution as long as it has the same size or smaller than the image of the entrance slit. It is therefore suitable to use an exit slit matching the image entrance slit and thereby get as much light as possible without affecting the resolution. In a diode array spectrometer the detector elements of the array are considered as exit slits and are often smaller than the entrance slit. Since the detector elements are next to each other no light is wasted even though the 'exit slits' are small. In this case a so called rolling mean[2] is taken for each element to reduce the influence of noise.

2.3.2 Imaging errors and diffraction

In ray- and wave optics one often considers lenses and mirrors to be parabolodial. The image of the entrance slit is at a distance L_B from the imaging optics which can be calculated using lens maker's formula:

[2]When a rolling mean is made, the value for each detector element is an average of the sampled value of that element and the adjacent ones (e.g. two elements at each side). As long as these elements don't have a total width larger than the entrance slit the FWHM increases very little.

$$\frac{1}{L_A} + \frac{1}{L_B} = \frac{1}{f} \tag{2.4}$$

where f is the focal length for the geometrical focus of the concave mirror or lens. Parabolodial mirrors are ideal for imaging systems but hard to manufacture. Instead spherical lenses and mirrors are used which are easier to produce and act similarly to their parabolodial cousins for paraxial rays[3] (see figure 2.6). For rays outside the paraxial region the differences between spherical and paraboldial lenses and mirrors increase which introduces imaging errors. Equation 2.4 will no longer be valid.

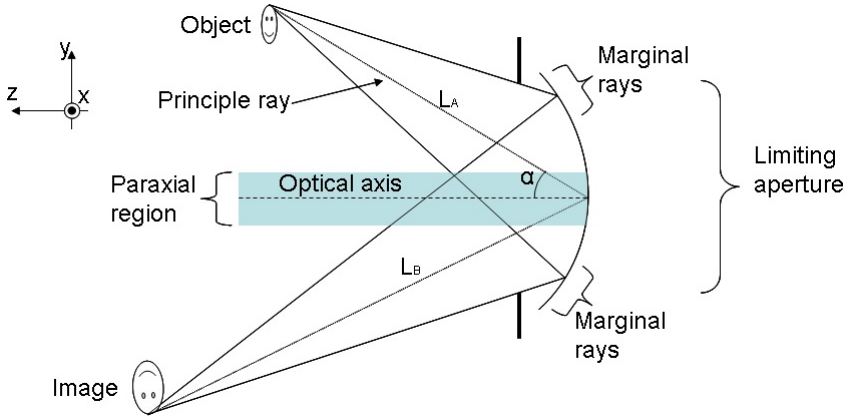

Figure 2.6: Imaging with a concave mirror. The principal ray is reflected at the centre of the limiting aperture.The magnification of the image is decided by the quote between the distances L_A (object to mirror) and L_B (mirror to image). The figure shows the tangential plane (perpendicular to the x-axis). If the sagittal plane should be observed instead (perpendicular to the y-axis) the incident angle α would appear to be zero.

Outside the paraxial domain the image is blurred by aberrations which can be modelled with Seidel theory [8]. These errors can be calculated by the function $W(\rho, \theta)$ which describe how a wave front is changed at the mirror. This function is an expansion of polynomials where each term represents a specific imaging error. These are described more in detail in appendix B. From Seidel theory a point spread function (PSF) can be calculated and the resulting image is given by convoluting the PSF with the original aberration free image. Seidel theory describes several different monochromatic aberrations. Some of them are: spherical aberration, coma, field curvature, distortion and astigmatism. They are explained below for a concave mirror where the limiting aperture coincides with the mirror itself (such as shown in figure 2.3).

Spherical aberration appears as a shift in focus for marginal rays from the geometrical focus. The marginal rays are focussed closer to the mirror, thus

[3]Paraxial rays travel nearly parallel to the optical axis and are incident close to the optical axis.

blurring the image of the entrance slit and broadening the spectrum. The magnitude of the spherical aberration is proportional to $(R^{-1} - L_B^{-1})$ where R is the radius of curvature of the concave mirror ($R = 2f$). This means that if the magnification $M = 1$ there is no spherical aberration.

Comatic aberration or coma has gotten its name from its look. A point imaged by an optical system suffering from coma has a comet like tail. Points of the objects far away from the optical axis (i.e. a high α in figure 2.6) are defocussed in the image plane because of varying magnification over the spherical mirror. The magnitude of coma is proportional to $(L_B - R)$. Like spherical aberration, there is no coma if the magnification $M = 1$.

If distortion is present in a system straight lines at the object are curved in the image. In ideal system the distance between the optical axis and different parts of the object is proportional to the distance between the optical axis and corresponding parts of the image. This is not the case if distortion is present. A square either gets the appearance of a barrel (barrel distortion), a pincushion (pincushion distortion) or a mix of both. This aberration is not present if a concave mirror, where the aperture coincides with mirror itself, is used for imaging.

Field curvature gives the image plane a curvature. For flat detector arrays this is a problem since only a small region can be in focus at the time. Field curvature is not present if a concave mirror, where the aperture coincides with mirror itself, is used for imaging.

Astigmatism is dependant on α^2 (incident angle). In an ideal optical imaging system there is only one focus. But in an astigmatic system the focal length in the tangential plane decreases while the focal length in the sagittal plane increases as α gets larger. This effect can be reduced in spectrometers where only resolution in one dimension is important (as in this thesis) by simply placing the exit slit/detector array at the correct focus.

Diffraction is not an optical aberration and does not depend on the geometry of setup in the same way as the aberrations described above, but can be treated as such. Diffraction is created from the limiting aperture. A small aperture gives a large Airy pattern. Diffraction differs from the aberrations described above since it is wavelength dependent and cannot be avoided.

The characteristic appearance of spherical aberration, coma, astigmatism and diffraction can be seen i figure 2.7. The aberration coefficients a_{nm}(described in appendix B) for the different imaging errors are here set to λ and the limiting aperture diameter was 10 mm. This would mean a broadening of A: 13 %, B: 3.2 %, C: 33 % and D: 2 % broader slit (if the image of the entrance slit would be 50 μm wide without aberrations or diffraction).

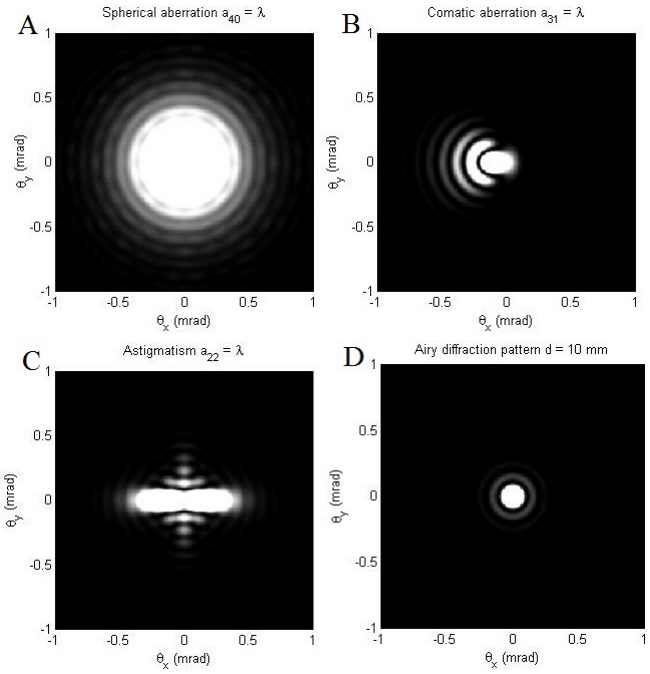

Figure 2.7: Example of A: spherical aberration, B: comatic aberration, C: astigmatism and D: Airy diffraction pattern.

2.4 Digital Micromirror Devices

A digital micromirror device (DMD) is a 2D-array of small mirrors used to direct light. It is found in applications such as medical science, optical networks and spectroscopy. There is a big market for DMD:s since a more recent application is Digital Light Processor (DLP) projectors. The ones used in this project were produced by Texas Instruments and can be found in several different configurations depending on the application.

2.4.1 Function

Each mirror is mounted on a hinge which goes between two opposite micromirror corners. By activating an electrode (yellow in figure 2.8) an electric field is created which turns the mirror towards it. By activating an electrode on the opposite side the mirror turns to that side. There are three states for each mirror; an 'on' state where the mirror is tilted $+12°$, an 'off' state where the mirror is tilted $-12°$ and a resting state where the mirror is more or less parallel with the DMD. The angles are decided by the geometry of the mirror mount. In this projected only the on and off states were used. The mircromirrors are mounted on a metal-oxide-semiconductor (CMOS) memory cell where either a logic '1' (on) or '0' (off) can be stored.

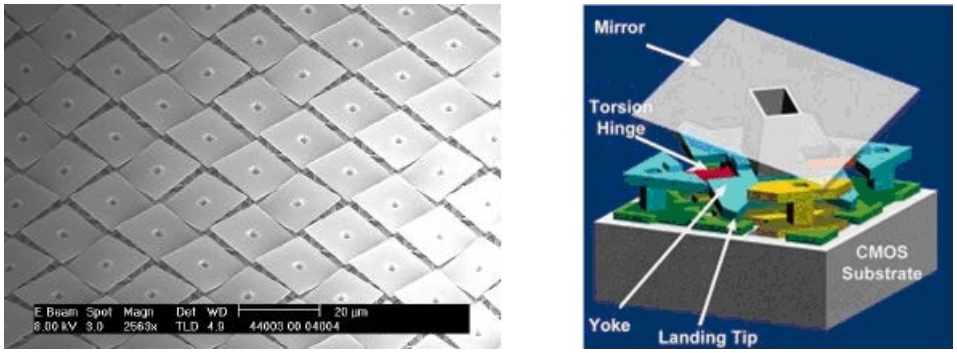

Figure 2.8: Principle of a DMD. When the electrode is charged it forces the mirror to tilt over its diagonal either right (up) or left (down) [10], [13].

2.4.2 DMD:s in spectrometers

There are two ways of using DMD:s in a spectrometer. One way of utilizing the DMD is put it where the detector array would have been placed in a detector array spectrometer, i.e. where the spectrum from the grating is focussed (see figure 3.1). The DMD reflects light, from the mirrors being on, into an optical fibre, detector or other configuration. The micromirrors will act as a reflecting exit slit. Even though they are not an actual exit slit they are referred to as such in this thesis. DMD:s can also be used as an imaging tool where the pixel(s) to be examined are chosen by the DMD and the spectrometer measures the intensity of the different wavelengths at that position. These are both examples that can be found patents [14] and published papers [13].

2.5 Hadamard spectroscopy

The most straightforward scheme for measuring a spectrum is by measuring one wavelength at the time by rotating a grating or sampling with different detector elements. When using a DMD this would mean that the micromirror columns of the DMD were turned on a couple at the time (e.g. first column 1-6, then 7-12, 13-18...) and thereby sweep the spectrum [4]. The measured values η_i can be written as,

$$\eta_1 = \psi_1 + e_1, \tag{2.5}$$
$$\eta_2 = \psi_2 + e_2, \tag{2.6}$$
$$\eta_3 = \psi_3 + e_3, \tag{2.7}$$
$$\eta_4 = \psi_4 + e_4, \tag{2.8}$$

where ψ_i is the actual value and e_i is the error. The expected value of the error $E(e_i)$ and the mean square error σ is:

$$E\left(\xi_i - \psi_i\right) = E\left(e_i\right) = 0, \tag{2.9}$$
$$E\left(e_i^2\right) = \sigma^2. \tag{2.10}$$

where $\xi_i = \psi_i + e_i$. The signal-to-noise ratio (SNR) is a quote which indicates how well the wanted signal can be resolved from noise,

$$SNR = \frac{\psi_i}{\sqrt{E\left(\left(\xi_i - \psi_i\right)^2\right)}}. \tag{2.11}$$

Another scheme to acquire a spectrum is Hadamard spectroscopy [4]. If all channels are used in a clever way, no signal is discarded. This is also called multiplexing. An example of how the channels can be combined is,

$$\eta_1 = \psi_1 + \psi_2 + \psi_3 + \psi_4 + e_1, \tag{2.12}$$
$$\eta_2 = \psi_1 - \psi_2 + \psi_3 - \psi_4 + e_2, \tag{2.13}$$
$$\eta_3 = \psi_1 + \psi_2 + \psi_3 - \psi_4 + e_3, \tag{2.14}$$
$$\eta_4 = \psi_1 - \psi_2 - \psi_3 + \psi_4 + e_4. \tag{2.15}$$

For sample j, η_j, the actual values at each channel i, ψ_i, are added according to a certain pattern[4]. For each sample j random noise, e_j, is included. The value of channel 1, ξ_1 can then be calculated:

$$\xi_1 = \frac{\eta_1 + \eta_2 + \eta_3 + \eta_4}{4} = \psi_1 + \frac{e_1 + e_2 + e_3 + e_4}{4} \tag{2.16}$$

The root mean square error is:

$$E\left(\left(\xi_1 - \psi_1\right)^2\right) = E\left(\frac{1}{16}\left(e_1 + e_2 + e_3 + e_4\right)^2\right) = \frac{\sigma^2}{4} \tag{2.17}$$

With four measurements, the average SNR is twice as high here compared to sweep spectroscopy. If the number of measurements increase to n the SNR raises $\sqrt{n}$ times. In practice matrices are often used:

$$\begin{pmatrix} \eta_1 \\ \eta_2 \\ \eta_3 \\ \eta_4 \end{pmatrix} = \begin{pmatrix} 1 & 1 & 1 & 1 \\ 1 & -1 & 1 & -1 \\ 1 & 1 & -1 & -1 \\ 1 & -1 & -1 & 1 \end{pmatrix} \begin{pmatrix} \psi_1 \\ \psi_2 \\ \psi_3 \\ \psi_4 \end{pmatrix} + \begin{pmatrix} e_1 \\ e_2 \\ e_3 \\ e_4 \end{pmatrix}$$

,

$$\eta = H_4\psi + e. \tag{2.18}$$

H_4 is a 4×4 Hadamard matrix which is optimal for these purposes [4]. But using 1's and -1's is not always a practical scheme in applications such as spectroscopy. It is more convenient to use 1's and 0's corresponding to transmitted/reflected and blocked light. In this project this corresponds to micromirrors

[4] In sweep spectroscopy $\eta_j = \psi_i$.

turned on or off. The best matrices in these conditions are so called S-matrices [4]. The masks for a 7×7 S-matrix (equation 2.19) can be seen in figure 2.10 and how it could be implemented in a Czerny-Turner spectrometer in figure 2.9.

$$S_7 = \begin{pmatrix} 1 & 0 & 1 & 0 & 1 & 0 & 1 \\ 1 & 1 & 0 & 0 & 1 & 1 & 0 \\ 1 & 0 & 1 & 1 & 0 & 1 & 0 \\ 1 & 1 & 0 & 1 & 0 & 0 & 1 \\ 0 & 1 & 1 & 0 & 0 & 1 & 1 \\ 0 & 0 & 0 & 1 & 1 & 1 & 1 \\ 0 & 1 & 1 & 1 & 1 & 0 & 0 \end{pmatrix} \tag{2.19}$$

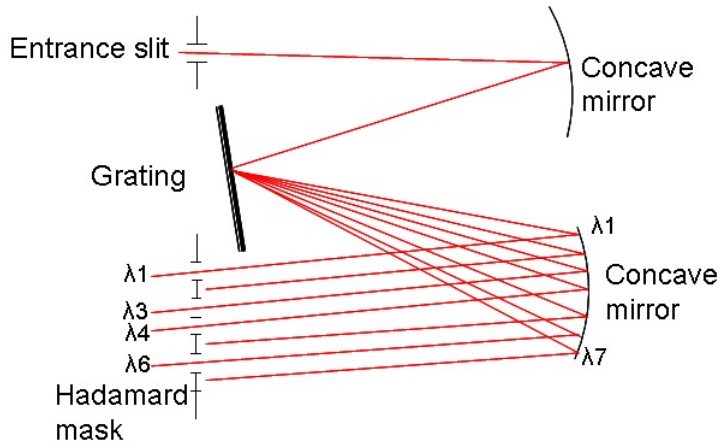

Figure 2.9: Example of Hadamard spectrometer, in a Czerny-Turner configuration with a 7×7 S-matrix (equation 2.19) as a mask at the exit. 7 masks are used corresponding to the 7 rows in S_7 (equation 2.19) with 1 sample at each mask. In this figure the third configuration (row 3).

An S-matrix S_{n-1} is constructed by taking a Hadamard matrix H_n and omitting the first row and column (thus creating an $(n-1) \times (n-1)$ matrix). All 1's are then replaced by 0's and all -1's replaced by 1's. In the examples above there are some condition that have to be fulfilled. The system must be detector limited[5] and all slits must have the same size. Using an S-matrix for multiplexing is only half as effective as an H-matrix. The SNR increases $\sqrt{n}/2$ times compared to sweep spectroscopy. Hadamard spectroscopy is explained more thoroughly in [4].

Decoding the measurements is done by simply multiplying the samples with the invers S-matrix:

$$\xi = S_n^{-1}\eta. \tag{2.20}$$

[5]In a detector limited system the noise is independent of the light intensity.

2.5.1 Hadamard spectroscopy with DMD:s

In the theory above a perquisites is that the all slits have the same size. When a mask with twice as many elements is used the mask is spatially twice as big. When a DMD is used as a Hadamard mask, by turning micromirrors on/off, half of the mirrors are always on. If S_{19} should be used as a Hadamard mask this would mean 19 slits composed of 25 micromirror columns each. S_{39} would in the same way mean 39 slits of 12 micromirror columns each. The total number of micromirrors that are on with each sample stays approximately the same. This means that the outgoing intensity is independent of the slit width. The intensity detected at each sample, η_j is

$$\eta_i \propto I_{tot}/2 \tag{2.21}$$

where each calculated measured channel value, ξ_i, is

$$\xi_i \propto \frac{I_{tot}}{n} \tag{2.22}$$

since there are n exit slits. The expected mean square error is

$$E\left((\xi_i - \psi_i)^2\right) = E\left(\frac{1}{n}\sum_{i=1}^{n} e_i\right) = \frac{\sigma^2}{n} \tag{2.23}$$

The mean square error decreases, but so does the signal. This means the the resulting SNR is then

$$SNR = \frac{\psi_i}{\sqrt{E\left((\xi_i - \psi_i)^2\right)}} = \frac{\frac{I_{tot}}{n}}{\sqrt{\frac{\sigma^2}{n}}} \propto \frac{1}{\sqrt{n}}. \tag{2.24}$$

This means that, even though the noise is decreased through multiplexing (as $2/\sqrt{n}$), the SNR decreases if the number of slits, n, increases (the signal is proportional to $1/n$). Multiplexing with a S_{19} matrix thus gives a twice as high SNR as a S_{79} matrix. It should also be taken into account that a S_{79} matrix demands 4 times as many samples. To get the same SNR with S_{79} as S_{19} a four times longer integration time is needed (if the same SNR is to be achieved). In total this gives a 16 times longer measuring time using S_{79} compared to S_{19}. Multiplexing still gives an SNR $\sqrt{n}/2$ times higher than using sweep spectroscopy (with the same slit width in a detector limited system).

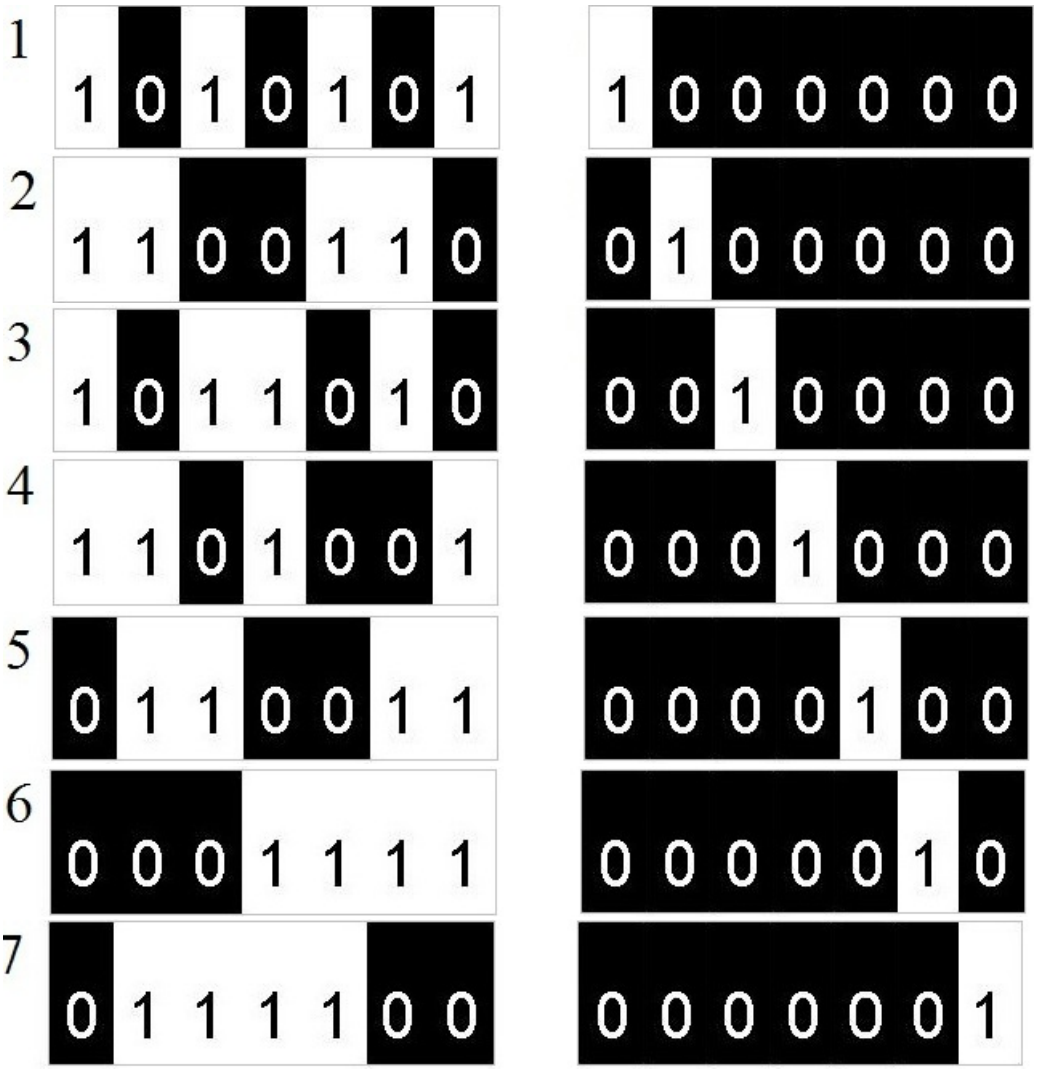

Figure 2.10: Examples of sweep (right) and Hadamard (left) masks. The Hadamard masks based on on a 7×7 S-matrix (equation 2.19). Slits marked with 1 transmit light, while slits marked with 0 block light.

Chapter 3

Setup

The aim of the optical setup, constructed during this thesis work, was to evaluate a pre-dispersive spectrometer design. This required optimization of the resolution while some other parameters (light throughput, detectors, size) requires more work continuing the project. The main design is described below but an alternative design was also evaluated. The second design is an extended version of the first one and is explained in appendix A.

3.1 Design

A schematic illustration of the setup used can be seen in figure 3.1. The light enters through a slit and is then split up spatially in its different wavelength components by a concave grating. The grating also images the entrance slit onto the micromirrors of DMD. The light is then focussed into an optical fibre using a lens and collimator.

This design can be used both as a pre- and post dispersive spectrometer (see section 2.1). In the first case, the spectrometer acts as a polychromator being able to choose a number of wavelengths only limited by the wavelength range of the incident light on the DMD and the DMD used. As a pre dispersive spectrometer the optical fibre could instead be coupled to the sample.

3.2 Grating

The grating is made by Horiba Jobin Yvon. It is a holographic grating with a groove density 370 grooves/mm. The grating was set up according to the parameters in table 3.1.

The best distance L_B was decided by measuring the FWHM of the spectrum while the DMD was moved towards the grating. It turned out that the best position was at $L_B = 113$ mm which is 16 mm closer to the grating than the geometrical image point at 129 mm. The focal length in the tangential plane vary with α and β according to [5]:

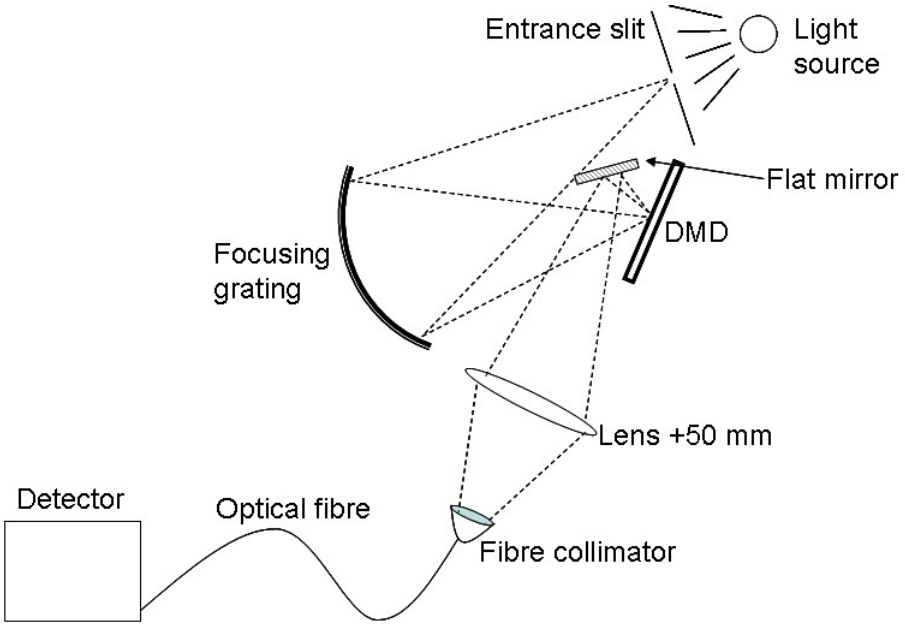

Figure 3.1: The setup. A detector has here been set at the exit.

$$f_T = f/cos(\theta) = \frac{R}{2} cos(\beta - \alpha) \approx 56mm \tag{3.1}$$

where f is the geometrical focal length. Using lens maker's formula (equation 2.4) an angle $\beta = 25°$ gives $L_B = 113$ mm, as in the optimized case. This means that the light is slightly better focussed for short wavelengths.

The setup used would give an ingoing and outgoing numerical aperture, $NA = sin(13.1°) \approx 0.23$[1]. It is however unclear how much of this incoming light was diffracted into the first order of the wavelength region of interest. It turned out that a major part of the grating could be covered without changing the intensity reaching the detector (with all micromirrors on). Of the grating area ($\approx 20cm^2$) only circa $0.8cm^2$ (10 mm in diameter) contributed to 80 % of the intensity of the spectrum (this varied somewhat in the wavelength region 850-1000 nm). This limits the numerical aperture to $NA = sin(2.6°) \approx 0.05$ and also the throughput. This limited effective grating size also effects resolution, using equation 2.2, $\partial\lambda$ can be calculated,

$$\partial\lambda = \frac{\lambda}{knW_g} = 0.25nm, \tag{3.2}$$

$\partial\lambda$ is equal to the FWHM or smallest distance between two resolvable peaks. It decreases/increases 0.02 nm when the wavelength is 850/1000 nm. To be able

[1] $arctan(\frac{L_B}{d/2}) = 13.1°$

L_A	110 mm
L_B	113 mm
R	118.73 mm
d	50 mm
α	5°
β_H	45°
$\beta(\lambda_1 = 850 \text{ nm})$	24°
$\beta(\lambda_n = 1000 \text{ nm})$	28°
Dispersion	22 nm/mm or 0.17 nm/micromirror

Table 3.1: Grating setup parameters (for parameter definitions see figure 2.3). It is worth noting that only a region 80 nm wide could be examined at the time.

to reach this limit an 11.4 μm narrow slit at the entrance and the DMD would be necessary (excluding any effects from diffraction or optical aberrations). Because of the low throughput at these conditions this limit was only tested but not used for measuring any spectra.

3.3 Imaging

The resolution of the spectrometer is, as discussed above, not limited by the resolving power of the grating. The entrance slit and generated exit slit on the DMD together with imaging errors dominates the broadening if not taken care of.

3.3.1 Slits

There are 2 slits in the design used in this project. The entrance slit is imaged onto the generated exit slit at the DMD by the concave grating. Together these two slits limit the resolution of the spectrometer. In the setup used in this project the entrance slit is magnified $M = L_B/L_A = 1.06$ times.

An exit slit which matches the entrance slit will give the highest throughput without sacrificing resolution. In sweep spectroscopy a rolling mean can be used in a very direct sense by first activating mirror 1-6, 2-7, 3-8, 4-9, etc. For each sample a sum is taken for the centre and adjacent micromirrors. This is not possible in Hadamard spectroscopy. On the other hand, the slit size will not affect the throughput as much using Hadamard as sweep spectroscopy (see section 2.5). The theoretically best possible resolution, not including any broadening processes, is 0.17 nm with only one micromirror column open.

Three different entrance slit widths were used in this project: 10, 50 and 200 μm. The exist slits were 6, 12 and 25 micromirrors wide (corresponding to 45, 91 and 189 μm) to fit Hadamard S-matrices of size 19, 39 and 79 rows and columns.

3.3.2 Imaging errors

Of the six principle aberrations described in section 2.3.2, three are present in the setup: spherical aberration, coma and astigmatism. Since the distance L_B and R are close to each other this limits the influence of spherical aberration and coma. Astigmatism is not diminished by the same conditions and is therefore dominating, as can be seen in the resulting PSF in figure 3.2. The aberration coefficients (which describe the magnitude of the errors, see appendix B) are $a_{40} = \lambda/1600$ (spherical aberration), $a_{31} = \lambda/18$ (coma) and $a_{22} = 1.3\lambda$ (astigmatism). At the tangential focus astigmatism does not effect the wavelength resolution. In table 3.2 the broadening for the different focusses is shown. It is clear that narrow entrance slits are more affected by aberrations than wide slits.

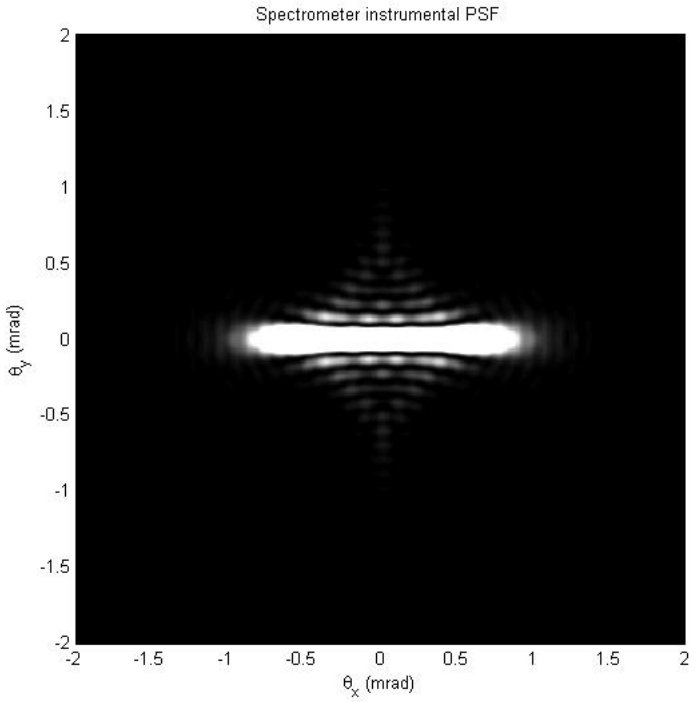

Figure 3.2: Resulting PSF from imaging errors and diffraction at the geometrical image point. The image is dominated by astigmatism.

It is worth noting that the three present aberrations all increase with a larger limiting aperture. The aberrations can be avoided by carefully choosing L_A and L_B and using the tangential image point. For a larger limiting aperture, a small change in L_B from the tangential focal point will increase the broadening of the spectrum severely.

Entrance slit width (μm)	FWHM (nm) Geometrical focus	Tangential focus	Aberration free
10	1.39	0.26	0.24
50	1.54	1.06	1.06
200	4.20	4.20	4.20

Table 3.2: Resulting imaging errors in one dimension (along the spectrum). The aberration free FWHM is still broadened by diffraction.

3.4 Optical fibre and detector

To evaluate the setup three different spectrometers were used at the exit (see table 3.3). Using spectrometers was an advantage since this gave direct information on what wavelength range was measured, the central wavelength for each micromirror column and how well the different wavelengths were directed into the optical fibre. The first one (USB2000) had a broad FWHM but needed less intense light than the other ones. USB2000 was used in the designing part of the project where resolution was not as necessary as a strong signal. The second (HR2000) had a better resolution but also needed more light. It was mainly used later in the project for testing the performance of the spectrometer. The last detector (AVASPEC) had a high resolution and was used for investigating the limits of the spectrometer designed in this project. This detector was only available for a limited time.

Model	Serial Number	Bandwidth	FWHM
USB2000	USB2G11251	825 - 1100 nm	4.5 nm
HR2000	HR2B911	825 - 1075 nm	1.8 nm
AVASPEC-2048TEC-USB2	0912048U1	600 - 1100 nm	0.8 nm

Table 3.3: Detectors used at the exit of the spectrometer.

The fibre was a 600 μm thick multimode fibre with a numerical aperture, $NA = 0.22$. The point of having an optical fibre at the exit is that it adds flexibility, but at the cost of lower throughput. The spectrometers described above could be changed by simply taking the fibre from one device to another. To make sure that all wavelengths were present, the fibre collimator was put at the image point from the lens. The light was focussed here which made sure that all wavelengths would enter the fibre. The wavelengths at the edges of the DMD had a lower intensity reaching the fibre end than the central wavelengths.

3.5 Digital Micromirror Devices in this project

The spectrometer measured the intensity difference between the two states on and off. In the ideal case the intensity at the off state is zero. The DMD:s (see figure 3.3) were taken from a DLP Developer's Kit from Texas Instruments. They were controlled using the already existing DLP hardware and using it as a second screen to a computer. Then the projector was instructed to show differ-

ent images of slits. The specifications for the DMD are shown in table 3.4 below.

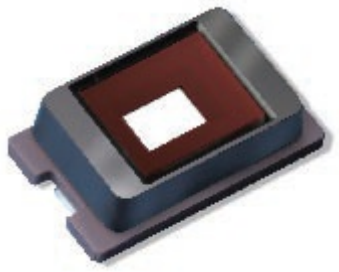

Figure 3.3: Digital micromirror device [15].

Resolution	480×320
Micromirror size	$7.56 \times 7.56 \mu m$
Tilt angle	$\pm 12°$
Array fill factor	92 %

Table 3.4: DMD specifications.

The DMD:s used are made for visible light and not near infrared. The single pass transmission through the window protecting the mirrors is circa 80 % in this region (compared to 92 % for visible light). Though there exists DMD:s with windows which transmit near infrared radiation well. Of the incoming light circa 55 % is reflected in the region 850-1000 nm (see figure 3.4).

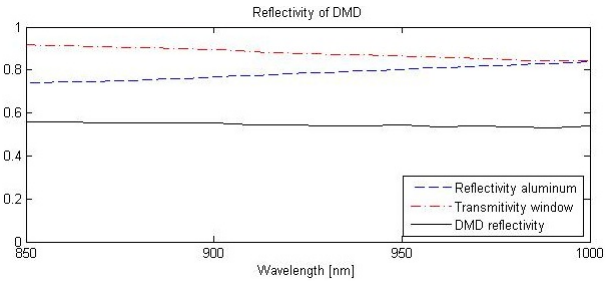

Figure 3.4: DMD reflectivity. The transitivity of the entrance window, reflectivity of aluminium and the micromirrors. The value for aluminium is taken from the reflectivity of Thorlabs aluminium mirrors [16]. The overall reflectivity of a DMD is around 55 % in the wavelength region 850-1000 nm.

3.6 FRED-simulations

The spectrometer was first modelled using the ray-tracing program FRED. A simple model was set up according to the specifications in the table 3.1. FRED was used to get a hint to which problems might occur and how optics should be placed. An advantage using FRED is that it can be run using scripts which allows simulation to be done where many components change properties (such as the micromirrors in the DMD during Hadamard spectroscopy). Since rays are used and each single ray only can consist of a discrete number of wavelengths and not a continuous spectrum this might either give errors or a long simulation time. Another drawback is that a full DMD with 480x320 mirrors take up to much computer power to have a usable model. Instead a 'DMD-like' component was used with 80x1 (each column correspond to 6x320 micromirrors) columns was used to get the program running smoothly. Also these columns directed all light either straight left or right (and not diagonally towards the corners like in a real DMD, see section 2.4.1). As in the experiment, astigmatism could be handled by positioning the DMD in the tangential focus at $L_B = 113$ mm. No other optical aberrations were observed. The simulated model could reconstruct a top hat spectrum perfectly well with Hadamard spectroscopy while sweep spectroscopy lacked in performance. This was not due to the method but rather to the discrete wavelengths. 100 different wavelengths were used.

Chapter 4

Method and Results

4.1 Measuring procedure

When measuring a spectrum two computers were used. Since the DMD:s were mounted in projectors, their hardware and software could used to control the DMD:s by telling them to project different pictures. One computer was used to control the projector using the software Microsoft PowerPoint 2003, through a HDMI output. Another computer was used for sampling values with one of the spectrometers at the exit. For each series of measurements a certain procedure was followed. First the background was sampled by displaying a black picture (all mirrors off). Secondly the full spectrum was sampled as reference by showing a white picture (all mirrors on). The spectrum was sampled through either sweep or Hadamard spectroscopy by displaying black pictures with white stripes corresponding to the wavelength(s) to be sampled (see figure 2.10). The width of the generated slits was determined by the width of the stripes. Afterwards the samples were treated using MatLab 7.10.0 (R2010a) to reconstruct the spectrum. To simulate how the spectrometer would react, if a single detector was used, all values in the USB2000/HR2000 measurement, in the wavelength interval of interest, were summed. This also sums noise from 550 channels which make a noisy detector. To reduce the influence of the noise a 'threshold level' TL was introduced. At e.g. TL = 5 all detector element samples, in the wavelength region of interest, with an amplitude higher than 5 were summed. This made the sweep measurements more reliable, while the Hadamard measurements were less affected (since half of the mirrors were open more channels detected light above TL). This filtering was used together with an ArHg lamp (see section 4.2) and a 50 μm narrow slit. The contribution from noise depend on the chosen threshold level. This might change the shape of of weak measured peaks. The only difference, in the measuring procedure, between sweep and Hadamard spectroscopy was that different pictures were displayed on the DMD and that the results from Hadamard spectroscopy needed to be decoded.

4.2 Light sources

To test the spectrometer and help while designing it, two different light sources were used: a halogen lamp and an argon-mercury (ArHg) lamp. Together these two light sources complement each other well. The halogen lamp has a continuum, even spectrum which stretches over the whole visible range into the infrared. This was a big help when setting up the spectrometer since the second order of visible, blue light is positioned at the same place as the invisible near infrared light examined in the project. This second order was blocked during the measurements by using a filter. To make sure that the spectrometer could not only resolve a broad, continuum spectrum the ArHg lamp was used. It has spectral lines of argon and mercury. The FWHM of these line were much thinner than 0.17 nm (the FWHM without aberrations, with only one micromirror column open). This proved to be a more difficult task than the halogen lamp since the ArHg lamp had a much lower intensity.

4.3 Sweep versus Hadamard spectroscopy

The first and most important result is that the spectrometer worked and could resolve a spectrum. In figure 4.1 the reconstructed spectrum from a halogen lamp. Both sweep and Hadamard spectroscopy were used here for different integration times (at HR2000 which was coupled to the exit) to test the limits of the designed spectrometer.

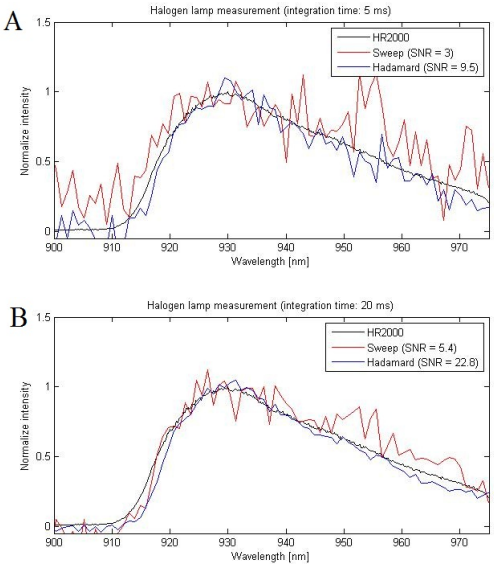

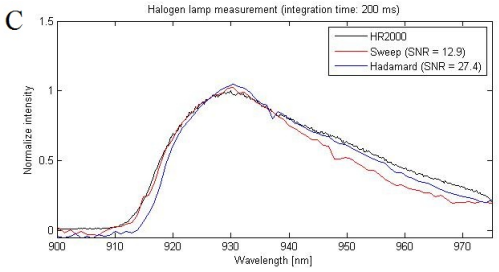

Figure 4.1: Comparison between Hadamard spectroscopy and sweep spectroscopy for different integration times, A: 5 ms, B: 20 ms and C: 200 ms. The reference spectrum in black is taken with HR2000 at the exit. It should be noted that it took just as long time to use the two different methods. The entrance slit was 50 μm wide while the generated slits at the DMD were 6 micromirrors wide. 79 samples were made (corresponding to an 79×79 S matrix).

In figure 4.1, a comparison between sweep and Hadamard spectroscopy has been done, where one can see that the Hadamard spectroscopy has a clearly better signal-to-noise ratio (see section 2.5). According to the theory it should be $\sqrt{79}/2 = 4.4$ times larger. In the results it's less: 3.2, 4.2 and 2.1 times (for A, B and C). An important factor that limits the performance of Hadamard spectroscopy is stray light. The DLP Developer's Kit (which contained the DMD) had internal LED:s which might have reached the detector. Parts of the setup such as rods, metal edges and frames might reflect incoming light in an unwanted way.

4.4 Measuring thin spectral lines

A continuous spectrum is easy to measure even with broadening processes present, while narrow spectral lines, as in in the ArHg lamp, are more difficult to analyse without changing the shape of the peaks. The ArHg lamp was used for testing the spectrometer (see figure 4.2). The light was analysed using a 50 μm (corresponding to circa 7 micromirrors) broad entrance slit together with a generated exit slit at the DMD 6, 12 and 25 micromirrors (corresponding to 45, 91 and 189 μm). Sweep spectroscopy was used.

The resolution is quite poor using a 25 micromirror wide exit slit while it turns out that the difference between 6 and 12 micromirrors is small. This is an important observation, since a wider exit slit gives a spectrum which takes shorter time to sample (39 samples with 12 micromirrors and 79 samples with 6 micromirrors). This is true as long as rolling mean is not used (see section 2.3.1). The full width half maximum was measured in two ways. In the first scheme, 6, 12 and 25 micromirrors exit slits were scanned using a rolling mean to examine the spectrometer resolution. This means that the number of samples remains the same for all exit slit widths. The result can be seen in figure 4.3. For the different exit slit widths the measured FWHM was 4.53 nm for 25 micromirror (theoretically 4.2 nm in a aberration free system), 2.43 nm for 12 micromirrors

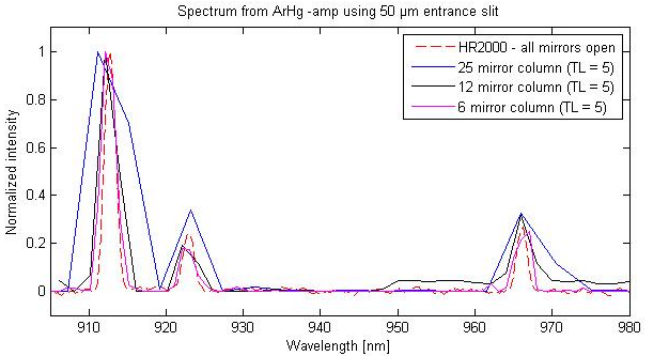

Figure 4.2: Comparison between different exit slit configurations on the DMD. 6, 12 and 25 micromirror columns were used (corresponding to 45, 91 and 189 ţm) in sweep spectroscopy. To reduce the noise a threshold level, TL, of 5 was used.

(theoretically 2.0 nm in a aberration free system) and 1.28 for 6 micromirrors (theoretically 1.0 nm in a aberration free system). To better resolve the peaks a threshold level of 10 was used. This especially affects the measurement with 6 mirrors and makes it appear thinner than it actually is. A more truthful value of the FWHM is 1.4 nm. The FWHM of the two other measurements remained unaffected. The entrance slit was 50 μm (7 micromirrors) wide.

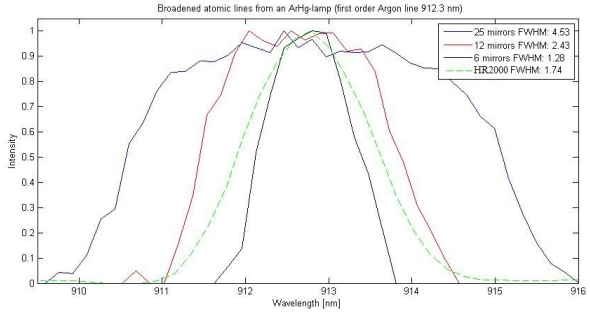

Figure 4.3: Resolution using a rolling mean.

4.5 Resolution limit

The relation between the FWHM and generated exit slit width was measured by expanding (instead of moving) the exit slit at the DMD one micromirror column at the time while keeping the entrance slit width constant at 10 μm. As predicted in the theory (see figure 2.5) the result, displayed in figure 4.4 shows a linear dependence of the FWHM on the width of the exit slit. The lowest value can be seen at 2-3 micromirrors (15-23 μm) which is about twice

as broad as the entrance slit. This measurement was done with a halogen lamp together with the detector AVASPEC which had a better throughput and resolution than both USB2000 and HR2000, which made this measurement possible.

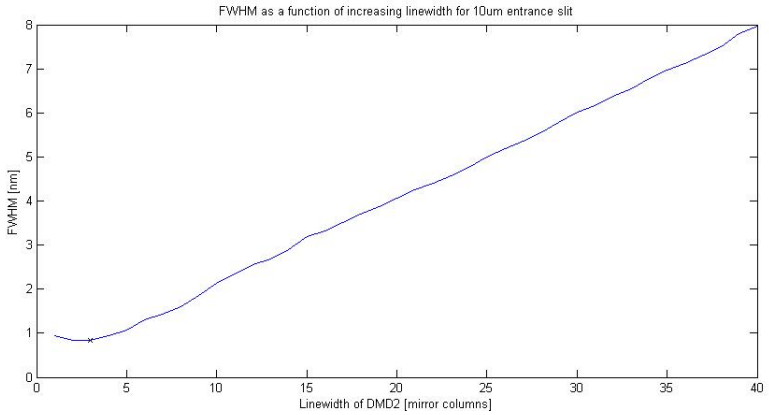

Figure 4.4: FWHM as a function of exit slit width. No threshold level reduction was used in these measurements.

As can be seen in figure 4.4 the minimum FWHM is 0.84 nm which is the limit of AVASPEC. This shows that the calculations for the imaging errors at the geometrical image point giving astigmatic effects were successfully avoided.

Chapter 5

Discussion and Conclusions

The first and most important conclusion is that a DMD can be used in a spectrometer as it has been in this project. This is a result which confirms already existing papers on this subject such as [15] and [13]. A problem in this project was low throughput which led to high levels of noise. Here Hadamard spectroscopy turned out to be a useful tool since it performed well when sweep spectroscopy had a high noise level. Multiplexing is a valuable asset when it can be as easily integrated into a system as it can in a DMD-based spectrometer. To use the setup with sweep spectroscopy a good detector at the exit is needed or a strong light source. Another option is to sacrifice resolution to get better intensity using wider entrance and exit slits or modifying the setup so that the throughput is increased. Only 5 % of the grating area was actually used which forced longer integration times.

If software was to be developed tailored for this setup the measurements could be made quicker and simpler. It would also open up for new features such as a self-evaluating system which could decide a well suited entrance slit depending on the spectrum, frequency modulating the mirrors and decoding with Fourier Transform or imaging using push-broom spectroscopy . It might also be possible to work around imaging errors by using other shapes on the DMD than rectangular slits.

This thesis could be something worth following up for FOSS when building spectrometers which operate in the near infrared region. Cheap DMD:s already exist which are designed for handling near infrared light. Since this is a young technology with a big market it is likely that it is likely to develop quickly. Larger DMD:s with more mirrors and windows suited for near infrared light are already available . The difficulties in this project were mainly because of low intensity, which depended on the grating, light diffracted to other orders and poor reflectivity of the DMD. Other difficulties came from inefficient software. Solving these problems would make the integration times shorter and the cost of the spectrometer would still be low.

Bibliography

[1] FOSS analytical, *Corporate brochure - Dedicated Analytical Solutions* found at http://www.foss.dk/Home/About%20Foss/About, visited December 30 2010.

[2] B.E.A. Saleh, M.C. Teich, *FUNDAMENTELS OF PHOTONICS* Second Edition, John Wiley & Sons, USA, 2007, chapter 4.4.

[3] Christopher Palmer, *Diffraction Grating Handbook*, sixth edition, found at http://gratings.newport.com/handbook/handbook.asp, visited February 7 2011, chapter 3 and 4.

[4] M.Harwit and N. J. A. Sloane, *Hadamard Transform Optics*, Academic Press, USA, New York, 1979, chapter 2.

[5] M.Harwit and N. J. A. Sloane, *Hadamard Transform Optics*, Academic Press, USA, New York, 1979, chapter 5.

[6] Sune Svanberg, *Atomic and Molecular Spectroscopy*, Fourth Edition, Springer-Verlag, 2004, chapter 6.6.2.

[7] http://www.astro.virginia.edu/class/oconnell/astr511/lec13-f03.pdf, visited January 2011.

[8] Virendra N. Mahajan, *OPTICAL IMAGING AND ABERRATIONS - PART I - RAY GEOMETRICAL OPTICS*, SPIE, Bellingham, Washington, 1998, chapter 3.

[9] Virendra N. Mahajan, *OPTICAL IMAGING AND ABERRATIONS - PART I - RAY GEOMETRICAL OPTICS*, SPIE, Bellingham, Washington, 1998, chapter 6.4.2.

[10] Michael R. Douglass, *DMD reliability: a MEMS success story*, SPIE, vol. 4980, USA, 2003.

[11] http://scien.stanford.edu/pages/labsite/2003/psych221/projects/03/pmaeda/, visited January 28 2011.

[12] J.M. Lerner and A Thevenon, *The Optics of Spectroscopy*, found at http://www.horiba.com/us/en/scientific/products/optics-tutorial//?Ovly=1, visited January 31, 2011.

[13] James D. Batchelor and Bradley T. Jones, *Development of a Digital Micromirror Spectrometer for Analytical Atomic Spectrometry*, Analytical Chemistry, vol. 70, No. 23, page 4907-4918, December 1 1998.

[14] Patent no:. US5,594,575 Ronald E. Stafford, Texas Instruments Incorporated, *SLM Spectrometer*, United States Patent, April 2 1996.

[15] NGUYEN THE QUYEN, EDOUARD DA SILVA, NGUYEN QUY DAO, and MICHEL D. JOUAN, *Raman Spectrometer Using a Digital Micromirror Device and a Photomultiplier Tube Detector for Rapid On-Line Industrial Analysis. Part I: Description of the Prototype and Preliminary Results*, Society for Applied Spectroscopy, vol 62, Number 3, France, 2008.

[16] Thorlabs, http://www.thorlabs.de/NewGroupPage9.cfm?ObjectGroup_ID=264, visited January 2011.

[17] Dana Dudley, Walter Duncan, John Slaughter, *Emerging Digital Micromirror Device (DMD) Applications*, SPIE, vol. 4985, Issue 14, Texas, 2003.

[18] THOMAS M. SPUDICH, CHARLES K. UTZ, JENNIFER M. KUNTZ, RICHARD A. DEVERSE, ROBERT M. HAMMAKER, and DAVID L. MCCURDY, *Potential for Using a Digital Micromirror Device as a Signal Multiplexer in Visible Spectroscopy*, Society for Applied Spectroscopy, Vol. 57, Number 7, USA, July 2003.

[19] Texas Instruments, *DLP 0.17 HVGA Chipset*, data sheet for the DLP from which the DMD was taken.

Acknowledgements

During my work designing and building many people have assisted me with encouragement, knowledge and skill. I would specially like to thank the following people:

head supervisor Dr. Erik Mansten,

assisting supervisor M.Sc. Senior Scientist Håkan Wedelsbäck,

examinator Dr. Hans Lundberg,

opponents Michele Giunta and Per Samuelsson,

all the helpful and encouraging people at both the Division of Atomic Physics at Lund University and FOSS in Höganäs.

and the coffee machines in both Lund and Höganäs which were always there in hard times.

Appendix A

Design 2

The difference between the original (design 1) and this alternative design (design 2) is that in the second design yet another DMD (DMD1 in figure A.1) is used. Its task is to act as an adjustable slit which adds more flexibility to the spectrometer (see figure A.1). In this design the light from the light from the entrance slit is focussed (and imaged) on DMD1 and from there reflected onto the grating. The slit could also be moved by simply changing the DMD micromirror configuration. To make this work the design in figure A.1 has to be modified since the light is focussed onto a small region of the DMD.

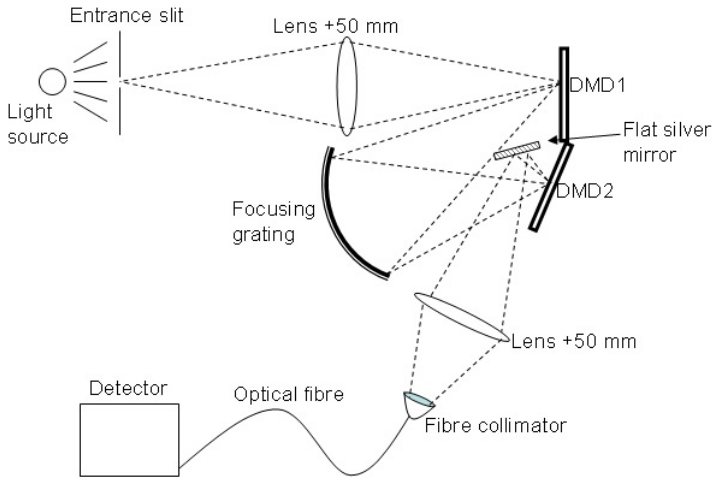

Figure A.1: The setup used for design 2.

Design 2 does in principle act the same way as design 1. The difference is that the generated slit at DMD1 has the same role as the entrance slit in design 1. It is important that the entrance slit (in design 2) is imaged onto DMD1. Otherwise the spectrum might be broadened because of overlapping images at DMD2.

As previously said, the DMD:s are designed for visible light (420-720 nm)

and have a lower reflectance in the in the near-IR range. This means that the throughout decreases with at least 45 % (see figure 3.4) as well as increasing the amount of stray light inside the spectrometer. Another factor is that the light from the entrance slit has to be focussed onto DMD1 which introduces more sources of error than in design 1.

Design 2 can, just as design 1, be used both as a pre- and post-dispersive spectrometer. In the first case high intensity isn't necessarily a problem since a strong light source can be used. In the second case the collecting components such as the entrance slit and lens are flexible and a good image at DMD1 isn't essential for the spectrometer. This makes it possible to collect light from a wide area and trough several entrance slits (instead of only using a single one as in figure A.1).

A.1 DMD1

In design 2 DMD1 introduces a defocussing imaging error not present in design 1. As can be seen in figure A.1 DMD1 is oriented perpendicularly to the principle ray of the incoming light from the entrance slit. This means that if the slit of open micromirrors should be moved, the distance between the slit and the grating (L_A in figure 2.3) changes maximum ± 1.8 mm. If the correct distance L_B is in the centre of DMD1 this means that the blur radius ρ_s of the image at DMD2 which can be calculated [2]:

$$\rho_s = \frac{1}{2} e L_B d, \tag{A.1}$$

where L_B is the distance between the grating and DMD2, d is the diameter of the limiting aperture and e is the focussing error:

$$e = \frac{1}{L_A} + \frac{1}{L_A} - \frac{1}{f}, \tag{A.2}$$

where L_A is the distance between DMD1 and the grating and f is the focal length of the concave grating. The blur diameter is maximum 68 μm which can be compared with a 50 μm wide slit used in the result. Another option would be to orient DMD2 facing the grating instead of perpendicular to the incoming light. Since astigmatism (which depends on α^2) was dominant imaging error this makes it hard to compensate for this error since the incident angle varies more.

A problem that occurs is diffraction. Since the mirrors are so small with spacing between them 7.56 μm there is a small but noticeable diffraction pattern after the incident light has been reflected by DMD1. If the DMD is seen as a grating, the mirror size is the distance between the grooves. This leads to a 7° diffraction angle with stray light which might create overlapping false spectrums. This effect becomes more significant if DMD1 is not oriented perpendicularly to the incident light. This effect was also present at DMD2 but did not affect the measurements notably.

Appendix B

Imaging errors for a concave mirror

A complete survey of Seidel theory is too extensive to include in this thesis. In this appendix follows a short summary of Seidel theory for a setup consisting of an object and a concave mirror producing an image of the object. The limiting aperture of the setup coincides with the mirror itself. A setup like the one used in this thesis.

When waves of light is transmitted or reflected from an object (such as light from an entrance slit or DMD) it spreads out in a cone. A distance away the wave fronts, emanating from each point of the object, forms a Fourier transform of the object. This makes it possible to manipulate the image of the light. By placing a concave, paraboloid mirror in front of this cone, it is reflected without obstructing the wave front much. The inverse Fourier transform is made and the object is reconstructed as an image. The image is blurred however, since the limiting aperture at the mirror forms an Airy pattern in the image plane. This is mathematically described as a convolution of the object and the Airy pattern [2].

As described in section 2.3.2, spherical mirrors are often used instead of paraboloidal mirrors. The change in shape means that the wave front at the mirror is not ideally reflected but instead obstructed by the mirror. Seidel theory [8] can describe this wave front error $W(\rho, \theta)$ by a series of polynomials:

$$W(\rho, \theta) = \sum_{n=1}^{\infty} \sum_{m=0}^{n} a_{nm} \rho^n cos^m(\theta). \tag{B.1}$$

If x_m and y_m are coordinates at the mirror plane then:

$$\rho = \frac{2}{d} \sqrt{x_m^2 + y_m^2}, \tag{B.2}$$

$$\theta = arctan\left(\frac{y_m}{x_m}\right). \tag{B.3}$$

where d is the diameter of the limiting aperture. Here follows calculations used in this thesis for the primary aberration terms. For a more accurate description

more terms (corresponding to higher n and m) can be added. Each aberration coefficient a_{nm} corresponds to an aberration (see table B.1).

n	m	Aberration Term	Aberration Name
1	1	$a_{11}\rho cos(\theta)$	Distortion
2	0	$a_{20}\rho^2$	Field curvature
2	2	$a_{22}\rho^2 cos^2(\theta)$	Astigmatism
3	1	$a_{31}\rho^3 cos(\theta)$	Comatic aberration
4	0	$a_{40}\rho^4$	Spherical aberration

Table B.1: Primary Seidel aberration polynomials [8].

As described in section 2.3.2 only spherical aberration, coma and astigmatism are present in this specific case. The wave front error can be calculated using following equations [9]:

$$W(\rho,\theta) = a_{40}\rho^4 + a_{31}\rho^3 cos(\theta) + a_{22}\rho^2 cos^2 cos(\theta), \tag{B.4}$$

$$a_{40} = \frac{1}{4R}\left(\frac{1}{R} - \frac{1}{L_B}\right)^2 \left(\frac{d}{2}\right)^4, \tag{B.5}$$

$$a_{31} = \frac{L_B - R}{R^2 L_B^2} L_A \alpha \left(\frac{d}{2}\right)^3, \tag{B.6}$$

$$a_{22} = \frac{1}{RL_B^2}\alpha^2 \left(\frac{d}{2}\right)^2. \tag{B.7}$$

The parameters are defined in figure 2.6. The point spread function (PSF) can be calculated [11]:

$$PSF(x,y) = \frac{1}{\lambda^2 d^2 A_{ap}} \left|\left| \mathcal{F}\left\{ p(\rho) \times e^{-i\frac{2\pi}{\lambda}W(\rho,\theta)} \right\} \right|\right| \tag{B.8}$$

$$p(\rho) = \begin{cases} 1 & \rho \leq 1 \\ 0 & otherwise \end{cases} \tag{B.9}$$

where $\mathcal{F}$ is the Fourier transform, A_{ap} is the area of the limiting aperture and $p(\rho)$ is the pupil function describing the transmission of the circular, limiting aperture. It is worth noting that if there are no aberrations present, the PSF is an Airy pattern of the limiting aperture. Even though Seidel theory gives a detailed description of optical aberrations such calculations are not to be fully trusted for a real setup. The information provided should be considered as a hint to how optics should be placed to avoid aberrations. To get good resolution, it has to be measured while parameters such as α, L_A and L_B are changed.